Optics & Laser Technology 161 (2023) 109232

Contents lists available at ScienceDirect

Optics and Laser Technology

journal homepage: www.elsevier.com/locate/optlastec

Full length article

Study of the processing conditions for stainless steel additive manufacturing using femtosecond laser

Iñigo Ramon-Conde [a,b], Ainara Rodriguez [a,b], Santiago M. Olaizola [a,b], Mikel Gomez-Aranzadi [a,b,*]

[a] CEIT-Basque Research and Technology Alliance (BRTA), Manuel Lardizabal, 15, Donostia / San Sebastián 20018, Spain
[b] Universidad de Navarra, Tecnun, Manuel Lardizabal, 13, Donostia / San Sebastián 20018, Spain

ARTICLE INFO

Keywords:
Femtosecond laser
Laser Powder Bed Fusion
Ultrashort pulse
Stainless Steel Powder
High precision manufacturing

ABSTRACT

The use of ultrashort-pulsed (USP) lasers in Additive Manufacturing (AM) enables the processing of different materials and has the potential to reduce the sizes and shapes manufactured with this technology. This work confirms that USP lasers are a viable alternative for Laser Powder Bed Fusion (LPBF) when higher precision is required to manufacture certain critical parts. Promising results were obtained using tailored and own-produced stainless steel powder particles, manufacturing consistent square layers with a series of optimized processing parameters. The critical role of processing parameters is confirmed when using this type of lasers, as a slight deviation of any of them results in an absence of melting. For the first time, melting has been achieved at low pulse repetition (500 kHz) and using low average laser power values (0.5–1 W), by generating heat accumulation at reduced scanning speeds. This opens up the possibility of further reducing the minimum size of parts when using USP lasers for AM.

1. Introduction

Additive Manufacturing has become one of the most promising fabrication technologies in recent years with various applications for different sectors [1–5] including those where high precision and resolution are essential, such as medical [6–9] or aerospace [10,11] sectors. As a result, the investment allocated to the transition from traditional (mainly subtractive) manufacturing processes to new AM technologies has increased notably [12]. Since they do not need auxiliary resources, these technologies enable an efficient use of materials, while leftover fabrication materials can be reused in subsequent processes [13]. Moreover, AM allows for a flexible production of customisable parts, as it enables changing the design or the constitutive material on the fly as requested by each application [14].

Commercially available AM systems are commonly based on continuous wave or long pulsed laser beams operating in the near infrared (800–1064 nm) [15]. This kind of lasers has enabled the production of metallic AM parts at low cost and with low emission of harmful gases and a short lead time [16,17]. However, these lasers still present certain drawbacks that must be overcome. Among these, the range of metallic materials that can be processed is quite limited, being stainless steel, titanium and aluminum the most common options [18–20]; this leaves a wide range of materials which are difficult to process with this type of lasers due to their high melting points or high reflectivity (e.g. tungsten [21] or copper [22,23], respectively). Apart from this, there are increasingly complex parts that require a better resolution than the one achieved with the aforementioned lasers [24], which normally require post-processing [25–27] to compensate the relatively poor dimensional accuracy and surface finish.

Comparing the different AM techniques used to manufacture metallic parts, Laser Powder Bed Fusion (LPBF) and other similar techniques (Selective Laser Sintering, Selective Laser Melting, etc.) offer the best results in terms of resolution and fabrication complexity [24,28], as their Maturity Index proves [29]. Analysing these techniques, the key role of the powder must be highlighted as it conditions the processing parameters and the quality of the fabricated parts [30]. In main industrial AM processes, the election of the powder is reduced to the powder formulas commercially available and accepted by the machine manufacturer. Despite the different possibilities, in many cases this selection is reduced to the most standard sizes used for LPBF and Direct Energy Deposition (usually between 30 and 150 μm), which narrows the choices [31,32]. To manufacture fine structures by means of

* Corresponding author.
E-mail address: mgomez@ceit.es (M. Gomez-Aranzadi).

https://doi.org/10.1016/j.optlastec.2023.109232
Received 25 August 2022; Received in revised form 2 December 2022; Accepted 27 January 2023
Available online 4 February 2023

AM both a small particle size and a low layer thickness are required, as they enable a more accurate control of the energy transmitted to the powder bed, achieving better results [33]. However, the application of finer powder formulas is more complicated due to their less flowability [34], making it difficult to achieve homogeneity when depositing powder layers.

An accurate selection of the process parameters enables the accumulation of heat, and therefore the melting of the powder bed. In order to obtain a controlled accumulation of heat in the processed area, not only is necessary to vary the laser power but also the scanning speed and the hatch distance. These two parameters control the number of pulses that reach the powder bed per surface unit area in the scanning direction and perpendicularly to it. A vast majority of industrial AM processes (using CW or long-pulsed lasers) create high-speed and relatively stable distribution of laser pulses in order to obtain a constant energy density value [35–38]; in doing so, the pulse overlap in every direction is kept constant.

Yet scarcely studied for additive manufacturing, USP lasers could be a novel approach to solve the aforementioned problems of material processing, specially in relation to the increase of the profile complexity. Femtosecond lasers have been used mainly for surface processing of multiple materials [39–45]. The Heat-Affected Zone (HAZ) is smaller than in other kind of lasers [46], making femtosecond lasers an ideal tool for surface processing and surface structuring applications by ablation, but not in principle for 3D AM, where melting is required [6].

When impinging the material, femtosecond laser pulses interact with it before heat diffusion takes place [47]. When laser pulses of such a short duration and low intensity interact with metallic targets, free electrons absorb the laser energy, involving thermalisation within the electron subsystem, energy transfer to the lattice, and energy losses due to heat transport from the electrons to the target [48]. This phenomenon is described by the two-temperature model [49]. When the laser intensity is high enough (just above the ablation threshold of the material), a dense, high temperature plasma is formed, while the remaining ions in the lattice of the material experience a strong Coulomb repulsion due to the charge inequality, and are removed from the material in a process known as Coulomb explosion [50,51]. For higher values of intensity, a more violent and explosive process takes place, known as phase explosion. In both cases, the deposited energy is used to ablate the material without an important increase in the temperature of the surrounding material [52].

Some authors have achieved the accumulation of significant amounts of heat onto various substrates using UPS lasers [53–55], so this opens up the possibility to accumulate enough energy to melt the substrate by maintaining low values of laser intensity. This means that femtosecond lasers could be a feasible option when a very controlled heat accumulation is needed, if the melting threshold can be reached without exceeding the ablation threshold, as shown in Fig. 1.

In contrast to continuous wave or long-pulsed lasers, USP lasers enable a more precise heat accumulation control, which leads to a more flexible melt pool; as a result, spatial resolution is enhanced, opening up the possibility of manufacturing finer and more complex structures [56], which may bring a great advance in metal AM for the previously mentioned industrial sectors, whose precision requirements tend to increase in complexity as time goes by. , the use of a smaller laser spot results in a higher accuracy, considerably less generation of debris during the process and a negligible HAZ outside the processing area (less thermal stress levels), which are important features for additive manufacturing. Additionally, the same femtosecond laser source could be used to improve the surface roughness (S_a) of the parts or even functionalize them, making the most of the all the capabilities that these lasers can offer. Nevertheless, as the heat diffusion dynamics take place in a time of a few picoseconds [35,57], the pulses must be delivered with a high frequency and a high spatial overlap to generate the desired heat accumulation, making the approach notably different from the standard AM with longer-pulsed lasers [58,59]. Thus, the process time will be longer compared to mainstream AM, which means a higher energy consumption and less production rates. Moreover, the cost of USP laser equipment is higher. Not only the laser system itself but also the optics and beam management devices, which need special coatings to avoid damage induced by the ultra-short high-energy pulses.

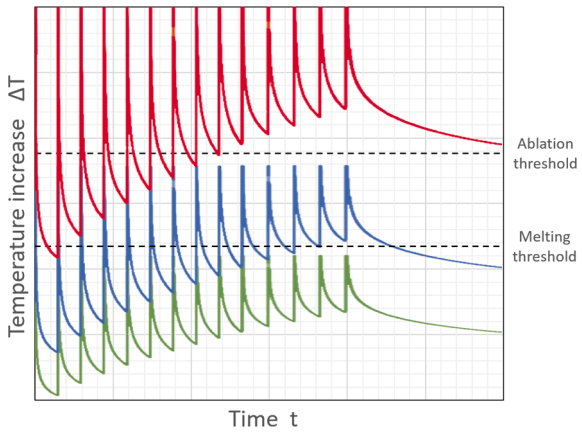

Fig. 1. Temperature evolution for different values of laser power: for power values too high (red), the temperature exceeds both the melting and ablation threshold, while for too low (green) power values, the temperature does not reach the melting threshold; for optimal power values (blue) the temperature is enough to melt the material but without triggering ablation. (For interpretation of the references to colour in this figure legend, the reader is referred to the web version of this article.)

Previous studies have demonstrated that the heat accumulation and melting of metal powders (such as iron [60], tungsten [60,61], copper [62] and aluminum [63]) is a feasible phenomenon when using USP lasers. These studies demonstrate that it is possible to melt various kinds of materials when laser pulses are consecutive enough, accumulating heat and increasing the temperature up to the melting threshold. Interestingly, to our knowledge, no studies have been carried out on stainless steel by any other author [64].

The present work focuses on achieving not only the melting of a stainless steel powder bed as the mentioned authors have done with other materials, but in obtaining an optimized melt pool to achieve a reduced roughness and a high material density, as a necessary step to build complex structures over it. This has been achieved studying the influence and optimizing the different processing parameters, and especially thanks to the access to own-atomized tailored stainless steel powder; the possibility in this case to self-produce low diameter metal powder to carry out the experiments added another parameter that normally cannot be controlled, and has been critical to the success of the process.

2. Material and methods

2.1. Setup

The irradiation source is a diode-pumped ultra-fast fibre laser system (Amplitude Satsuma HP) of $\lambda = 1030$ nm and 280 fs pulse duration, with a maximum average power of 10 W at a repetition rate of 500 kHz.

The properties of the laser beam (i.e., laser power, pulse repetition, polarization and spot diameter) are modified and controlled by the different modules of the micromachining setup (LASEA LS-Lab). Finally, an F-theta lens focuses the laser beam to a 29.9 μm diameter spot on the processing area. The spot location on the sample is controlled using a scanning head inside the micromachining setup, which enables to process an area of up to 60 × 60 mm without moving the stage.

In order to evaluate both the quality of the melting and the characteristics of the fabricated structures, the samples were analysed by different imaging techniques including optical microscopy (LEICA M205

FA) and Scanning Electron Microscopy (SEM) (ZEISS SIGMA and JEOL JSM 7100F). Moreover, by means of a 3D Optical Profiler (Sensofar S Neox) the roughness (Sa) of all the samples was calculated following the ISO 25178 standard, to quantify the quality of the obtained structures.

2.2. Materials

Ceit is able to produce tailored metal powders for AM [65]; taking advantage of this, own-produced gas atomized metallic powder grains have been used. Two different powder sizes have been selected in order to study the effect of the powder size as an additional variable, named coarse powder (20–45 μm size distribution) and fine powder (<20 μm size distribution) to differentiate between them, and shown in Fig. 2. The size of the particles was selected based on two aspects: a. the size of the spot diameter, so it can cover the maximum grain surface; b. the values found in literature, which were below 50 μm [60,62,63]. The chemical composition of these powders is presented in the following table (Table 1), which corresponds to an AISI 316L stainless steel. The powder was kept in a vacuum drier at room temperature to prevent moisture absorption.

AISI 304L stainless steel cut into slabs of 125 × 100 × 5 mm was selected as a substrate to deposit the powder and carry out the processes. All the experiments were carried out inside a processing chamber filled with argon to prevent oxidation during the laser irradiation.

2.3. Methods

2.3.1. Powder application procedure

In order to generate a layer with a reproducible thickness, as a first step we studied how to apply the powder onto the substrate. Mimicking LPBF powder application systems, a series of blades with controlled recesses were created. The gaps generated in the blades ranged from 50 to 200 μm in steps of 25 μm. The powder was manually deposited on the AISI 304L stainless steel platform and it was extended perpendicularly to the stage by means of the coating blades.

To overcome the expected deposition problems of the fine powder, the surface of the substrate was first treated with laser to increase its roughness and therefore enhance the substrate-powder adherence. After the laser ablation process, the profile of this treated area was analysed using a 3D Optical Profiler (Sensofar S Neox), obtaining a S_a of 3.3 μm and a depth of 51.499 μm. The first layer was applied onto this area using a blade without any recess, making the powder fill the ablated volume. The following layers were applied using the collection of blades with increasing recess mentioned above, resulting in structures with a thickness up to 250 μm.

Using this application procedure homogeneous layers were obtained: in the case of the coarse powder 100 and 200 μm layers and in the case of fine powder 50 μm layers. A sketch of the powder application process with the blades is shown in Fig. 3.

2.4. Laser process

In order to define the limits of the process, the first target was to find the ablation limit of the powder, which was expected to vary slightly from the bulk material. Therefore, the starting point for all the parameters was set taking in to account the ablation threshold of bulk stainless steel [47,66]. The power was varied between 0.34 and 2.03 W, the scanning speed between 2.5 and 100 mm/s and the hatch distance between 2.5 and 50 μm. Although the power used in our experiments was low compared to other laser sources used in literature [60–63,67], we supposed that the shorter duration of the pulses and the high repetition rate would enable the laser to reach the required energy to trigger the desired powder melting. This was the case so, once the ablation threshold was found, an independent study of the different parameters was performed in order to analyse the effect of each of them and with the main goal of producing regular powder melting. The values used to study each parameter are displayed in Table 2.

A linear laser polarization parallel to the processing direction was used in all the tests. Regarding the scanning strategy, it was adapted to the use of USP lasers. In mainstream AM, the strategy usually consists in using a fast scanning speed to overlap rapidly the subsequent lines and generate a stable and uniform melting pool in a relatively broad area. In this case, the strategy was directed to obtaining a good melting in each of the lines scanned with the laser. The main reason for this is that, in this case, due to the slower speed needed to melt the powder and to the significantly lower heat incubation capacity of the femtosecond pulses, it was not possible to obtain a melted area broader than each single line.

This way, the idea was to sequentially overlap independently melted lines scan by scan to conform the whole layer. The distance between processed lines was not fixed initially, since the efficiency of the melting process was not known with total precision. Depending on the amount of powder melted in each line, two strategies were considered in order to have a good melting in relation to hatch distance:

If the heat accumulation was high enough to melt the powder both below the irradiated area and its surroundings, the chosen hatch distance needed be larger than the spot diameter, having no overlap between laser scanning lines.

If the heat accumulation was not enough to melt the whole irradiated area, an overlap between scanning lines was needed to achieve a complete melting of the powder, and therefore the hatch distance would be lower than the spot diameter. In this second case, the percentage of overlap between scanning lines determines the amount of remelted area, and hence, the quality of the melt.

3. Results and discussions

The results have been divided in various sections, in order to explain the effect of each parameter. As all of them are interrelated, their adjustment has been done tuning them successively, starting with the laser power.

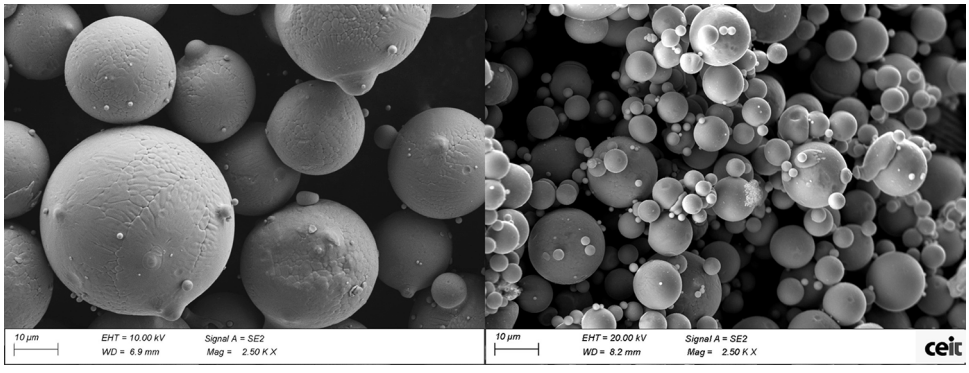

Fig. 2. SEM images of coarse powder (left) and fine powder (right).

Table 1
AISI 316L Stainless Steel composition.

Element	C	Si	Mn	P	S	Cr	Ni	N	Mo	Fe
% Present	0.03	1.00	2.00	0.045	0.015	16.5–18.5	10.00–13.00	0.10	2.00–2.50	Balance

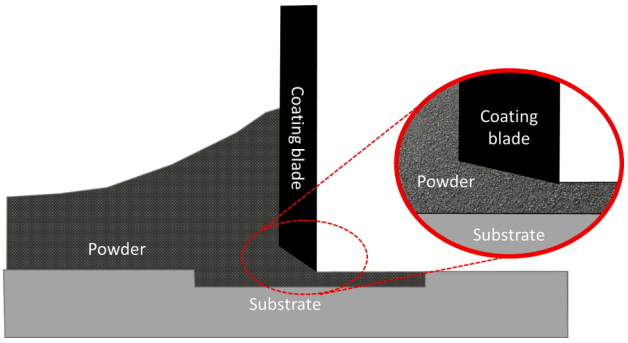

Fig. 3. Sketch of the powder application process of the first layer onto the laser treated area.

Table 2
Processing parameter list.

Parameter	Laser Power [W]	Scanning Speed [mm/s]	Hatch Distance [μm]	Layer Thickness [μm]
Laser Power study	0.34–2.03	2.5–50	10–50	50–200
Scanning Speed study	0.65–0.935	1–12.5	5–10	50
Hatch Distance study	0.65–0.935	2.5–5	2.5–10	50

3.1. Laser power

Laser power has been the most influencing parameter on the results. As stated before, the main challenge when using this type of lasers for AM is to transfer the high energy of the femtosecond laser pulses to melt the metallic powder while at the same time avoiding ablation, which occurs if the power is too high and/or it is delivered in an incorrect rate. If ablation happens, it can be found either in the powder particles or in the substrate; the later results in the expulsion of the grains from the processing area to the surroundings of the ablated area, as it is shown in Fig. 4 a) to c).

By decreasing the power from the maximum acceptable value below the ablation regime, a relatively quick transition has been observed from a completely ablated substrate to an absence of any effect at all on the substrate or the powder (Fig. 4). This is in close agreement to the values found by Groenendijk and Meijer [66] in their experiments. This transition is also present when using longer pulses, but in the case of femtosecond pulses the process window is significantly narrower [48,68].

Nevertheless, this proves that a window exists in which femtosecond laser pulses are able to melt stainless steel powder. In our case, this window has been found for both coarse and fine powder, and its narrowness underscores the critical role of the laser power. The experiments made with the coarse powder succeeded in melting the powder particles between values of power of 0.3 W and 0.6 W. The number of particles melted was enough to generate a layer with a thickness of 150–200 μm (Fig. 5, left), which is slightly lower than the thickness of the applied powder layer. As it can be seen in Fig. 5 (right), these melted layers have a core of melted metal with unmolten particles attached to their surface. Despite the melting generated between particles, the accumulated heat did not reach the lower levels of each layer; hence, the powder did not attach to the substrate. For higher values of power, as mentioned before, the melt was not improved and, furthermore, ablation occurred.

The experiments made with the fine powder also found a lower limit below of which the powder is not affected. In this case, below 0.5 W the result was similar to the one observed in Fig. 4-d) for coarse powder. When the power was increased above this value the powder started to melt and the particles agglomerated forming bigger spheres. Increasing the power further from 0.62 W to 0.85 W, the melting was enhanced and the agglomerated spheres increased in size and increased in quantity. As a result, these big particles joined each other and a more uniform and smoother surface was obtained; this can be see in Fig. 6, where the increase of power reduces slightly the S_a from 3.45 μm to 2.58 μm. In addition to this, melting occurred both between the powder particles and between the particles and the substrate, which was a significant advance comparing to the results obtained with the coarse powder.

In order to improve the powder melting and once the power value was set, a good combination of the other parameters (scanning speed and hatch distance) was sought. This is explained in the following sections.

3.1.1. Powder size

One of the effects seen when the fine powder melted was that the overall volume the particles occupied in the powder bed decreased. This made the surrounding powder particles collapse and fall into the melt track. Due to this, the surrounding area was slightly lower after the process, modifying slightly the conditions. This phenomenon, known as denudation, has already been studied as one of the defects present in LPBF processes [69,70]. In the case of the coarse powder, unless the power was excessively high, no denudation or any other unusual phenomena was perceived.

When analysing the melted area, it was observed that fine powder particles were properly melted in stable structures with a relatively smooth surface and good quality. Stable melt occurred also with the substrate, due to the thinness of the layers and the smaller powder size,

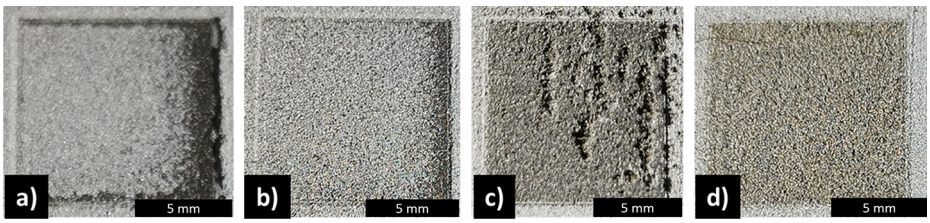

Fig. 4. Power influence on 1x1 cm^2 coarse powder processes: 2.03 W (a), 1.35 W (b), 0.68 W (c) and 0.34 W (d); scanning speed of 50 mm/s and hatch distance of 50 μm. The darker areas seen in pictures from a) to c) correspond to areas where powder particles have been ejected.

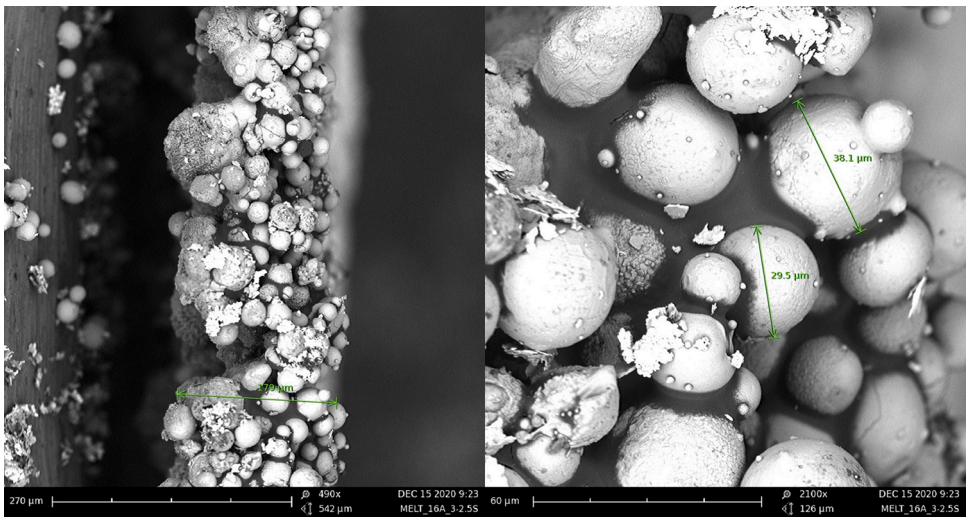

Fig. 5. Monolayer structure created with coarse powder particles (left), internal molten metal core with unmolten particles attached to the surface (right).

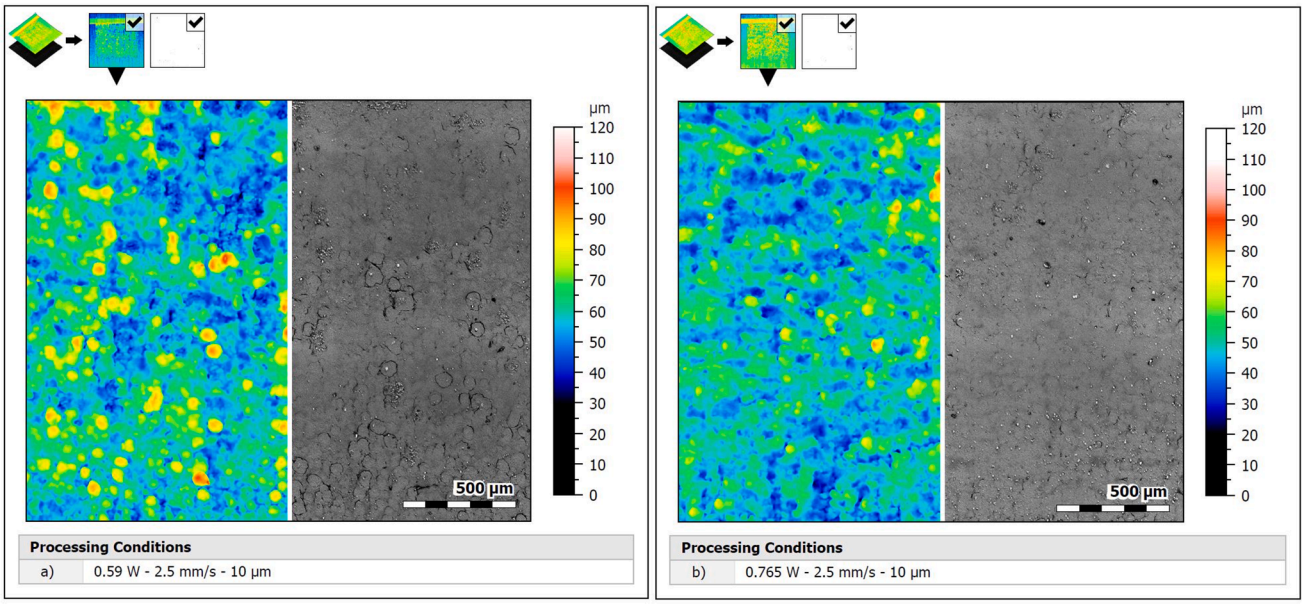

Fig. 6. Influence of power variation in fine powder: samples processed with a laser power of 0.59 W (a) and 0.765 W (b), a scanning speed of 2,5 mm/s and a hatch distance of 10 µm. The S_a values are 2.58 µm and 3.45 µm, respectively.

which contributed to generate a strong bond in the powder-substrate interface. When using coarse powder, the particles also melted forming stable structures with a granular and rough surface; nevertheless, the powder was not completely melted from top to bottom of the layer due to the thickness of the layers. Therefore, no efficient powder-substrate melt occurred. The melting between the substrate and the fine powder may need higher energy values to take place, which explains the fact that the optimal laser power window for the fine powder was higher than for the coarse powder.

As the results obtained with the fine powder were better in terms of roughness and substrate-powder melting, the coarse powder was discarded for the process of tuning the remaining parameters, and only the fine powder was used.

3.1.2. Scanning speed

In order to generate the desired heat accumulation, not only the energy of the pulses, but also the amount of pulses per surface unit area is a crucial parameter. The scanning speed, together with the hatch distance, are the parameters that control this pulse accumulation per area.

For the optimization of the scanning speed, the values optimized in the previous section were used as a starting point. The laser power was first tuned to the lower end of the window process, using values of 0.68 W and 0.765 W, and the scanning speed was decreased from 5 mm/s down to the lowest possible value. The first tests were performed with a power value of 0.68 W. As the number of pulses per unit of area increased, the accumulated heat grew, melting the metal powder and making powder particles attach to each other, forming bigger particles by coalescence. In Fig. 7, where the scanning speed is reduced from 5 mm/s to half of its value, an increase in the size of the particles can be observed, generating larger powder agglomerates in the process area. This size increase translates to an increase of the S_a, from 5.43 µm to 6.75 µm. On the contrary, for the experiments performed at 0.765 W the reduction of the scanning speed gave as a result a slight reduction of the S_a, from 6.89 µm to 6.49 µm, as in this case there was not a significant increase in the size of the melted agglomerates. Further reduction of the

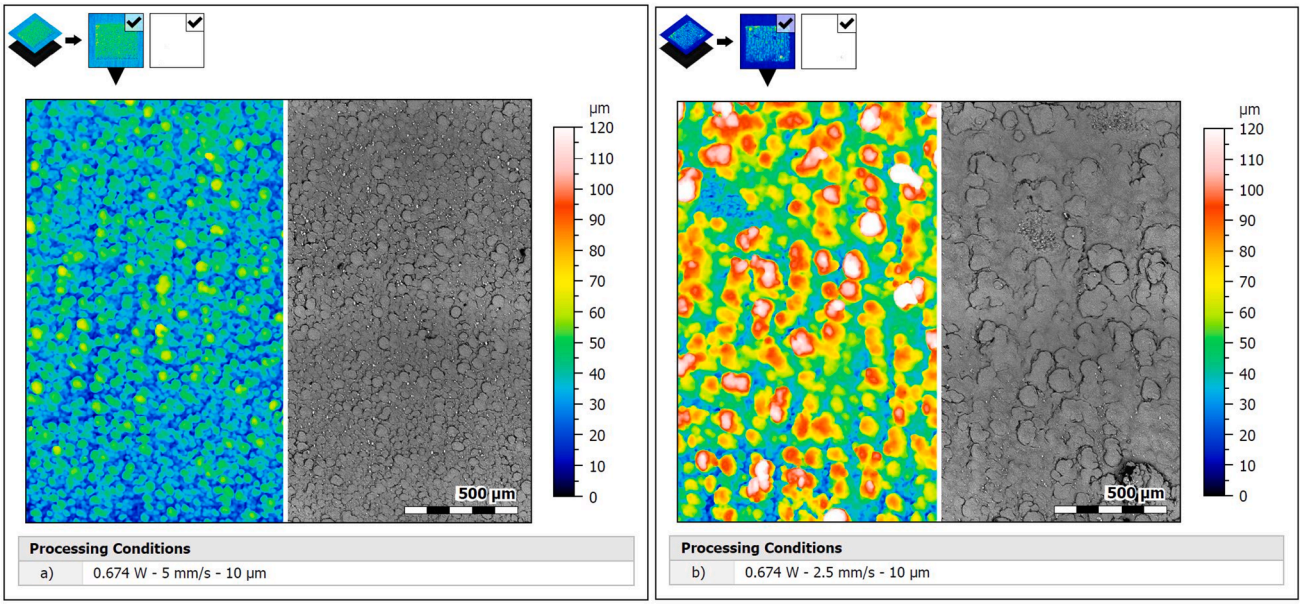

Fig. 7. Influence of scanning speed variation: samples processed with a laser power of 0.674 W and a hatch distance of 10 μm. When the scanning speed is reduced from 5 mm/s (a) to 2,5 mm/s (b), the S_a value increases from 5.43 μm to 6.75 μm.

scanning speed led to better results at both power levels, decreasing the S_a value down to 3.9–4.1 μm. This is because as the speed decreases, the agglomerates tend to coalesce in a layer, forming a more uniform structure.

After this, it was decided to test the highest laser powers inside the previously defined process window, with values ranging from 0.85 to 0.935 W. The same experiments were repeated, but now the starting point for the scanning speed was 2.5 mm/s. In this case the S_a decreased even more sharply, down to 3.5–3.8 μm. These results are shown in Fig. 8. It is worth mentioning that, in the minimum positively tested value of the scanning speed (1.5 mm/s), the obtained S_a value was inversely proportional to the value of the laser power. Below this minimum value, in all the samples the pulse accumulation exceeded the damage threshold, causing the breaking and burning of the melted powder; analogue results were obtained by Mizoshiri et al. [71] where at a constant fluence and a decreasing scanning speed (from an initial value of 5 mm/s), the particles were sintered instead of fully melted.

As a conclusion, it was observed that the optimal hatch value that leads to well-melted structures corresponds to a speed of 1.5 mm/s, while the variation of the power (always inside the predefined process window) does not have a significant effect in terms of roughness. All these tests were done with a hatch distance of 10 μm, which could affect

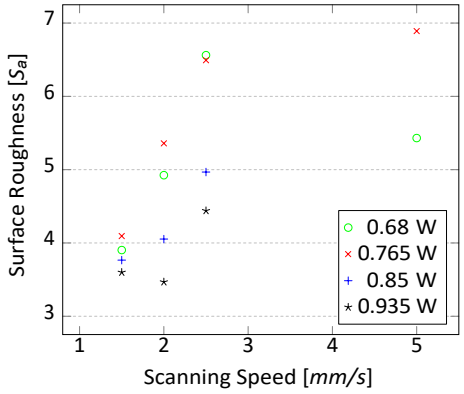

Fig. 8. Influence of the scanning speed on the surface roughness for different laser power values and a hatch distance of 10 μm.

this conclusion due to the interrelation between the different parameters.

As a more general conclusion, it can be concluded that the scanning speed has a very strong influence on the process, as only for a specific window of scanning speed values the accumulation of heat is enough to melt the powder and create a proper layer. Above this optimal window, the pulses cannot cause sufficient heat accumulation in the powder to create a stable melt, and they are only able to melt few powder particles; below it, the consecutive pulses affect negatively the powder bed and the structures formed by the previous pulses.

To further optimise the process, the influence of the hatching distance was studied, as shown in the next section.

3.2. Hatch distance

When optimising the hatch distance, the first factor taken into account was that in all the previous processes the melted area was smaller than the spot size. This seems reasonable, as the Gaussian distribution of the energy means that the central area of the spot concentrates most of the energy of the pulse. This was the main reason to choose an initial hatch distance of 10 μm to tune the previous parameters.

To confirm that to further optimise this parameter a reduction rather than an increase was more suitable, an initial test was done increasing the hatch distance to 20 μm, higher than the previous value but still smaller than the spot diameter. The result can be seen in Fig. 9. In Fig. 9 (left), the scanning direction can be inferred by the alignment of the melted agglomerates along the vertical axis. In contrast to this, due to smaller distance between scanning lines, in the image of the right no signs of scanning lines are observed; a more uniform melt is obtained with the lower hatch distance, therefore improving the quality of the surface.

As a result, it was decided to decrease the value of the hatch distance below 10 μm as a means to try to find a more optimised result.

As observed in Fig. 10, when the hatch distance was lowered further, and always inside the processing window defined in previous sections, the increase in the surface quality was even more pronounced. Decreasing the hatch distance value from 7 to 5 μm had a clear influence in the quality of the melt; this is evident in the reduction of the value of S_a from 6.75 μm in Fig. 10 a) to 4.1 μm in Fig. 10 b). In line with what has been said before, if the amount of accumulated heat is not enough to

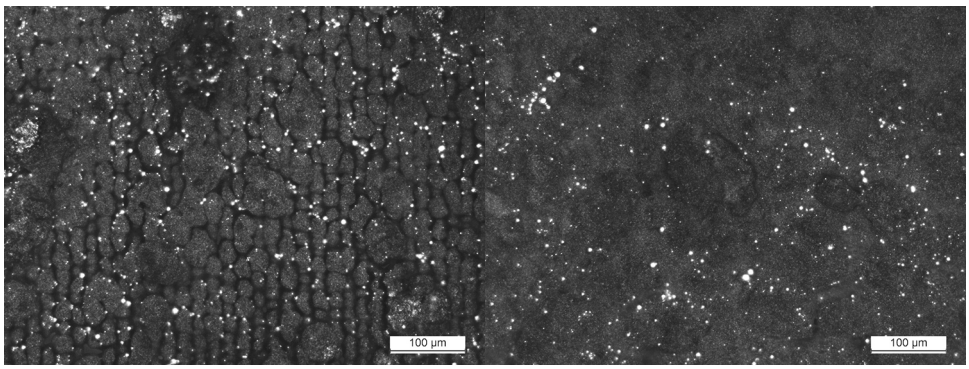

Fig. 9. Effect of the variation of the hatch distance from 20 µm (left) to 10 µm (right), for a sample processed with a laser power of 0.76 W and a scanning speed of 2.5 mm/s.

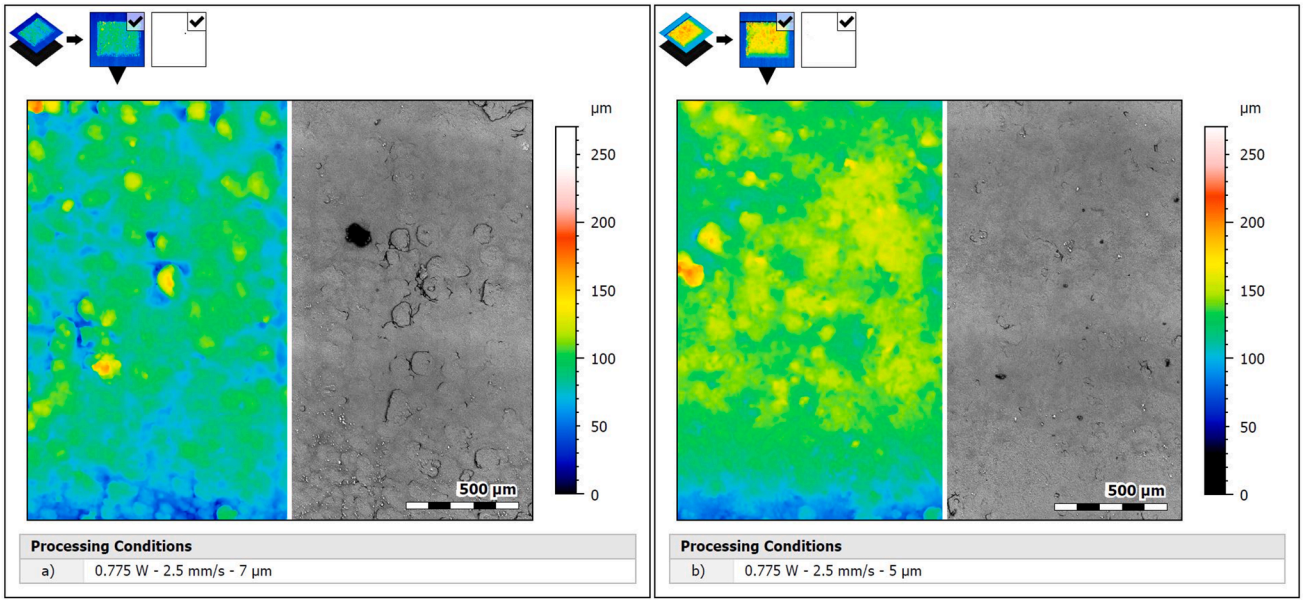

Fig. 10. Effect of the hatch distance reduction: samples processed at 0.775 W, 2.5 mm/s and hatch distance of (a) 7 and (b) 5 µm; traduced in a decrease of the S_a value from 6.75 µm to 4.1 µm.

melt uniformly the powder particles, various imperfections appear. This is shown in Fig. 10 a), where the powder is melted and agglomerated in spheres of around 100 µm in diameter in some areas, which affects the quality of the melt.

The improvement of the melted structure quality was observed for different laser power values as the hatch distance was reduced, as Fig. 11 depicts. For different processes carried out inside the optimal power and scanning speed window, the surface roughness decreases down to a value of 2–3 µm. The scanning speed value was shifted up to 2.5 mm/s from last section's results due to the interrelation between parameters and their sometimes antithetical effects: since the hatch distance reduction triggers a higher heat accumulation in the process area, the scanning speed was increased to compensate this heat accumulation excess per unit area.

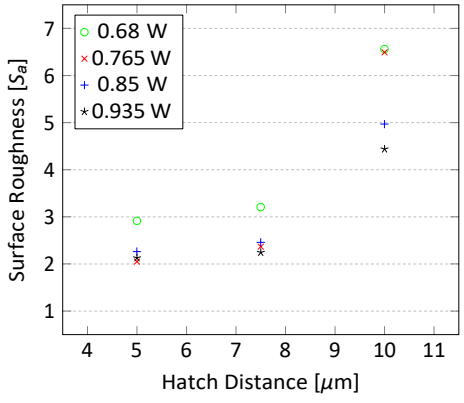

Fig. 11. Hatch distance variation influence on S_a for different laser power values and a scanning speed of 2.5 mm/s.

Although these results highlight the extreme difficulty of accumulating heat by means of femtosecond laser pulses, relatively smooth and uniform structures were obtained by decreasing the hatch distance to values where the overlap between lines exceeded the 80 %. High overlap values were also used in other processes for both accumulating heat in the process area and achieving a good surface finish [72–74].

Knowing that the pulse repetition rate is 500 kHz, the pulse-to-pulse distance in the Y-axis (scanning direction) can be calculated, which corresponds to a value of 5 µm. Interestingly, the best results were obtained for hatch distances between 5 µm and 7.5 µm, which means that the pulse overlap values are equal -or almost equal in both X and Y directions. Fig. 12 shows that, when using the optimal processing parameters, a very smooth surface with a very uniform melting can be obtained, reaching a S_a average value of 2.37 µm.

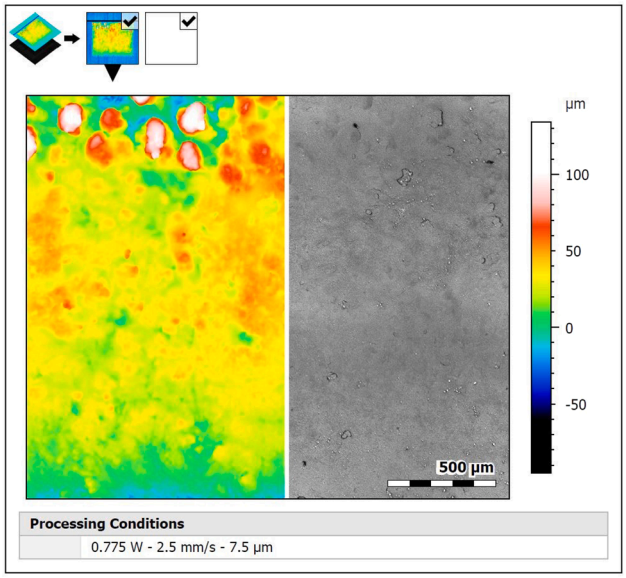

Fig. 12. Processing conditions that gave the best additive manufacturing results in our experiments: laser powder of 0.775 W, scanning speed of 2,5 mm/s and hatch distance of 7,5 µm; with a S_a average value of 2.37 µm.

Despite this, various imperfections can be observer in the top-left area of the sample. This could be due to certain irregularities present on the substrate, or that the distribution of powder is not exactly the same throughout all the area. As a result, when the sample is cleaned these "irregular" areas are damaged or removed from the surface, but the rest of the sample maintains the smooth finish observed just after processing.

4. Conclusions

In order to study the potential of ultra-short pulse lasers in additive manufacturing, a femtosecond laser was used as energy source in LPBF processes, performing different studies with two different sized and own-produced stainless steel powder types. After studying the different parameters, the first conclusion is that laser power is the most critical one, as an excessive energy transmitted to the powder results in ablation. Once an operative power window was found for the laser power, in which the powder and substrate were melted without signs of ablation, the values of scanning speed and hatch distance were optimized to achieve a uniform and smooth surface.

As a result of this optimization, the best results corresponded to the following processing conditions:

All tested values of laser power between 0.775 W and 0.935 W allow for the melting of powder. For these values, as the both the hatching distance and scanning speed decrease the surface roughness decreases. Although the lowest surface roughness was initially obtained with a minimum scanning speed of 1.5 mm/s, the optimal scanning speed value has been definitely set to 2.5 mm/s when considering the interdependence between all the parameters.

The value of hatch distance that gives the best result depends on the selected power value, although its variation is relatively small. For the lowest power inside the process window, the optimum hatch distance is 5 µm, while for the highest power, this value is 7.5 µm.

Compared to the laser sources found in industrial systems, the use of a femtosecond laser means a more complex laser-matter interaction and an increased challenge to produce heat accumulation due to the use of ultra-short energetic pulses. As a result, the optimal scanning speeds are notably lower that mainstream LPBF procedures. In contrast to this, it has been proven that the spatial distribution of heat is controlled more precisely, enabling us to fabricate well-melted stainless steel structures.

Furthermore, these results were obtained using laser powers and pulse repetition rates lower than any other author, achieving melting below 1 MHz and with average power levels below 1 W [62,63,67,71,75,76].

Finally, it is worth mentioning the remarkable variations in processing parameters that can be found in literature regarding the processing of metallic powder with UPS lasers, while in standard AM manufacturing they tend to be quite constant. The main reason for this is that, as two new parameters such as pulse repetition and pulse duration are added to the process, multiple possibilities arise in terms of parameter combinations for each material [64].

Declaration of Competing Interest

The authors declare that they have no known competing financial interests or personal relationships that could have appeared to influence the work reported in this paper.

Data availability

Data will be made available on request.

Acknowledgements

Authors would like to acknowledge the CDTI and the Spanish Ministry of Science and Innovation for the funding received for the CEFAM Project under the awarding and funding program for Excellent Technology Centers 'Cervera' (CER 20191005).

References

[1] C. Kai Chua, C. How Wong, W. Yee Young, Introduction to 3D Printing or Additive Manufacturing, Standards, Quality Control, and Measurement Sciences in 3D Printing and Additive, Manufacturing (2017) 1–29, https://doi.org/10.1016/B978-0-12-813489-4.00001-5.

[2] K. Vanmeensel, K. Lietaert, B. Vrancken, S. Dadbakhsh, X. Li, J. P. Kruth, P. Krakhmalev, I. Yadroitsev, J. Van Humbeeck, Additively manufactured metals for medical applications, Elsevier Inc., 2018. http://doi.org/10.1016/B978-0-12-812155-9.00008-6.

[3] A. Ostendorf, A. Neumeister, S. Dudziak, S. Passinger, J. Stampfl, Micro- and nano-parts generated by laser-based solid freeform fabrication, Adv. Laser Mater. Process.: Technol. Res. Appl. (2010) 695–734, https://doi.org/10.1533/9781845699819.7.695.

[4] S. Rahmati, Direct Rapid Tooling, in: Comprehensive Materials Processing 10, Elsevier, 2014, https://doi.org/10.1016/B978-0-08-096532-1.01013-X.

[5] I. Gibson, D. Rosen, B. Stucker, M. Khorasani, Additive Manufacturing Technologies, Addit. Manuf. Technol. (2021) 623–647, https://doi.org/10.1007/978-3-030-56127-7.

[6] N. Maharjan, W. Zhou, Y. Zhou, Y. Guan, N. Wu, Comparative study of laser surface hardening of 50CrMo4 steel using continuous- wave laser and pulsed lasers with ms, ns, ps and fs pulse duration, Surface and Coatings Technology 366 (November 2018) (2019) 311–320. http://doi.org/10.1016/j.surfcoat.2019.03.036.

[7] V. Finazzi, A.G. Demir, C.A. Biffi, F. Migliavacca, L. Petrini, B. Previtali, Design and functional testing of a novel balloon-expandable cardiovascular stent in CoCr alloy produced by selective laser melting, J. Manuf. Processes 55 (March) (2020) 161–173. http://doi.org/10.1016/j.jmapro.2020.03.060.

[8] A. Sarker, M. Leary, K. Fox, Metallic additive manufacturing for bone-interfacing implants, Biointerphases 15 (5) (2020) 050801, https://doi.org/10.1116/6.0000414.

[9] C. Gao, C. Wang, H. Jin, Z. Wang, Z. Li, C. Shi, Y. Leng, F. Yang, H. Liu, J. Wang, Additive manufacturing technique-designed metallic porous implants for clinical application in orthopedics, RSC Adv. 8 (44) (2018) 25210–25227, https://doi.org/10.1039/c8ra04815k.

[10] B. Blakey-Milner, P. Gradl, G. Snedden, M. Brooks, J. Pitot, E. Lopez, M. Leary, F. Berto, A. du Plessis, Metal additive manufacturing in aerospace: A review, Mater. Des. 209 (2021), V, https://doi.org/10.1016/j.matdes.2021.110008.

[11] M. Kamal, G. Rizza. Design for metal additive manufacturing for aerospace applications, Elsevier Inc, 2019, https://doi.org/10.1016/B978-0-12-814062-8.00005-4.

[12] V. Schmidt, M.R. Belegratis. Biological and Medical Physics, Biomedical Engineering Laser Technology in Biomimetics Basics and Applications, Springer, Berlin, Heidelberg, 2013, https://doi.org/10.1007/978-3-642-41341-4.

[13] B. Sartin, T. Pond, B. Griffith, W. Everhart, L. Elder, E. Wenski, C. Cook, D. Wieliczka, W. King, A.M. Rubenchik, S. Wu, B. Brown,C. Johnson, J. Crow, 316L POWDER REUSE FOR METAL ADDITIVE MANUFACTURING, 2017.

[14] S.H. Huang, P. Liu, A. Mokasdar, L. Hou, Additive manufacturing and its societal impact: A literature review, Int. J. Adv. Manuf. Technol. 67 (5–8) (2013) 1191–1203, https://doi.org/10.1007/s00170-012-4558-5.
[15] E.C. Santos, M. Shiomi, K. Osakada, T. Laoui, Rapid manufacturing of metal components by laser forming, Int. J. Mach. Tools Manuf. 46 (12–13) (2006) 1459–1468, https://doi.org/10.1016/j.ijmachtools.2005.09.005.
[16] V. Madhavadas, D. Srivastava, U. Chadha, S.A. Raj, M.T.H. Sultan, F.S. Shahar, A. U.M. Shah, A review on metal additive manufacturing for intricately shaped aerospace components, CIRP J. Manuf. Sci. Technol. 39 (2022) 18–36, https://doi.org/10.1016/j.cirpj.2022.07.005.
[17] A. Selema, M.N. Ibrahim, P. Sergeant, Metal additive manufacturing for electrical machines: Technology review and latest advancements, Energies 15 (2 2022). http://doi.org/10.3390/en15031076.
[18] D. Herzog, V. Seyda, E. Wycisk, C. Emmelmann, Additive manufacturing of metals, Acta Mater. 117 (2016) 371–392, https://doi.org/10.1016/j.actamat.2016.07.019.
[19] S. Gorsse, C. Hutchinson, M. Gouné, R. Banerjee, Additive manufacturing of metals: a brief review of the characteristic microstructures and properties of steels, Ti-6Al-4V and high-entropy alloys, Sci. Technol. Adv. Mater. 18 (1) (2017) 584–610, https://doi.org/10.1080/14686996.2017.1361305.
[20] B. Wu, Z. Pan, D. Ding, D. Cuiuri, H. Li, J. Xu, J. Norrish, A review of the wire arc additive manufacturing of metals: properties, defects and quality improvement, J. Manuf. Process. 35 (August) (2018) 127–139, https://doi.org/10.1016/j.jmapro.2018.08.001.
[21] A. Talignani, R. Seede, A. Whitt, S. Zheng, J. Ye, I. Karaman, M.M. Kirka, Y. Katoh, Y.M. Wang, A review on additive manufacturing of refractory tungsten and tungsten alloys, Addit. Manuf. 58 (2022) 103009, https://doi.org/10.1016/j.addma.2022.103009.
[22] B. David, selektives laserschmelzen von kupfer und kupferlegierungen, Fraunhofer-Institut fur Lasertechnik LTI, 2014. Ph.D. thesis.
[23] M. Colopi, L. Caprio, A.G. Demir, B. Previtali, Selective laser melting of pure cu with a 1 kW single mode, fiber laser 74 (2018) 59–63, https://doi.org/10.1016/j.procir.2018.08.030.
[24] D. Behera, S. Chizari, L. A. Shaw, M. Porter, R. Hensleigh, Z. Xu, X. Zheng, L.G. Connolly, N.K. Roy, R.M. Panas, S.K. Saha, X.R. Zheng, J.B. Hopkins, S.C. Chen, M. A. Cullinan, Current challenges and potential directions towards precision microscale additive manufacturing – Part IV: Future perspectives, Precision Engineering 68 (December 2020) (2021) 197–205. http://doi.org/10.1016/j.precisioneng.2020.12.014.
[25] T.D. Ngo, A. Kashani, G. Imbalzano, K.T. Nguyen, D. Hui, Additive manufacturing (3D printing): A review of materials, methods, applications and challenges, Compos. B Eng. 143 (2018) 172–196, https://doi.org/10.1016/j.compositesb.2018.02.012.
[26] W.E. Frazier, Metal additive manufacturing: A review, J. Mater. Eng. Perform. 23 (2014) 1917–1928, https://doi.org/10.1007/s11665-014-0958-z.
[27] D. Ding, Z. Pan, D. Cuiuri, H. Li, Wire-feed additive manufacturing of metal components: technologies, developments and future interests, Int. J. Adv. Manuf. Technol. 81 (2015) 465–481, https://doi.org/10.1007/s00170-015-7077-3.
[28] A. Vyatskikh, S. Delalande, A. Kudo, X. Zhang, C.M. Portela, J.R. Greer, Additive manufacturing of 3D nano-architected metals, Nature, Communications 9 (1) (2018), https://doi.org/10.1038/s41467-018-03071-9.
[29] AM-Power-Report, Metal additive manufacturing technology, last accessed 3 November 2022 (2022). URL https://additive-manufacturing-report.com/additive-manufacturing-metal-technology/.
[30] C. Meier, R. Weissbach, J. Weinberg, W.A. Wall, A.J. Hart, Critical influences of particle size and adhesion on the powder layer uniformity in metal additive manufacturing, J. Mater. Process. Tech. 266 (2019) 484–501, https://doi.org/10.1016/j.jmatprotec.2018.10.037.
[31] P. Sun, Z.Z. Fang, Y. Xia, Y. Zhang, C. Zhou, A novel method for production of spherical ti-6al-4v powder for additive manufacturing, Powder Technol. 301 (2016) 331–335, https://doi.org/10.1016/j.powtec.2016.06.022.
[32] A.M. Rausch, M. Markl, C. Körner, Predictive simulation of process windows for powder bed fusion additive manufacturing: Influence of the powder size distribution, Comput. Mathem. Appl., 78 (7) (2019) 2351–2359, simulation for Additive Manufacturing. https://doi.org/10.1016/j.camwa.2018.06.029.
[33] M. Sinico, A. Witvrouw, W. Dewulf, Influence of the particle size distribution on surface quality of Maraging 300 parts produced by Laser Powder Bed Fusion, Proceedings of the Special Interest Group meeting on Advancing Precision in Additive Manufacturing (2019) 31–34. euspen.
[34] S.E. Brika, M. Letenneur, C.A. Dion, V. Brailovski, Influence of particle morphology and size distribution on the powder flowability and laser powder bed fusion manufacturability of Ti-6Al-4V alloy, Addit. Manuf. 31 (2020) 100929, https://doi.org/10.1016/j.addma.2019.100929.
[35] T. Larimian, M. Kannan, D. Grzesiak, B. AlMangour, T. Borkar, Effect of energy density and scanning strategy on densification, microstructure and mechanical properties of 316L stainless steel processed via selective laser melting, Mater. Sci. Eng. A 770 (June 2019) (2020) 138455. http://doi.org/10.1016/j.msea.2019.138455.
[36] Č. Donik, J. Kraner, I. Paulin, M. Godec, Influence of the energy density for selective laser melting on the microstructure and mechanical properties of stainless steel, Metals 10 (7) (2020) 1–19, https://doi.org/10.3390/met10070919.
[37] T. Ullsperger, D. Liu, B. Yürekli, G. Matthäus, L. Schade, B. Seyfarth, H. Kohl, R. Ramm, M. Rettenmayr, S. Nolte, Ultra-short pulsed laser powder bed fusion of Al-Si alloys: Impact of pulse duration and energy in comparison to continuous wave excitation, Addit. Manuf. 46 (March 2021), https://doi.org/10.1016/j.addma.2021.102085.
[38] J.P. Choi, G.H. Shin, M. Brochu, Y.J. Kim, S.S. Yang, K.T. Kim, D.Y. Yang, C.W. Lee, J.H. Yu, Densification behavior of 316L stainless steel parts fabricated by selective laser melting by variation in laser energy density, Mater. Trans. 57 (11) (2016) 1952–1959, https://doi.org/10.2320/matertrans.M2016284.
[39] A.Y. Vorobyev, C. Guo, Direct femtosecond laser surface nano/microstructuring and its applications, Laser Photon. Rev. 7 (3) (2013) 385–407, https://doi.org/10.1002/lpor.201200017.
[40] M. Martinez-Calderon, A. Rodriguez, A. Dias-Ponte, M.C. Morant-Miñana, M. Gomez-Aranzadi, S.M. Olaizola, Femtosecond laser fabrication of highly hydrophobic stainless steel surface with hierarchical structures fabricated by combining ordered microstructures and LIPSS, Appl. Surf. Sci. 374 (2016) 81–89, https://doi.org/10.1016/j.apsusc.2015.09.261.
[41] M. Martinez-Calderon, M. Manso-Silván, A. Rodriguez, M. Gomez-Aranzadi, J. P. Garcia-Ruiz, S.M. Olaizola, R.J. Martin-Palma, Surface micro- and nano-texturing of stainless steel by femtosecond laser for the control of cell migration, Sci. Reports 6 (July 2016) 1–10, https://doi.org/10.1038/srep36296.
[42] A. San-Blas, M. Martinez-Calderon, J. Buencuerpo, L. M. Sanchez Brea, J. del Hoyo, M. Gomez-Aranzadi, A. Rodriguez, S.M. Olaizola, Femtosecond laser fabrication of LIPSS-based waveplates on metallic surfaces, Appl. Surf. Sci. 520 (January) (2020) 146328. http://doi.org/10.1016/j.apsusc.2020.146328.
[43] C.S. Chang, C.K. Chung, J.F. Lin, Surface polishes of the SKD 61 tool steel by a femto pulse laser operating in a wide range of powers, J. Mater. Process. Technol. 277 (1) (2020) 116465, https://doi.org/10.1016/j.jmatprotec.2019.116465.
[44] Y. Zhao, H. Liu, T. Yu, M. Hong, Fabrication of high hardness microarray diamond tools by femtosecond laser ablation (2021). http://doi.org/10.1016/j.optlastec.2021.107014.
[45] P. Bizi-Bandoki, S. Valette, E. Audouard, S. Benayoun, Effect of stationary femtosecond laser irradiation on substructures' formation on a mold stainless steel surface, Appl. Surf. Sci. 270 (2013) 197–204, https://doi.org/10.1016/j.apsusc.2012.12.168.
[46] K. Sugioka, Y. Cheng, Ultrafast lasers-reliable tools for advanced materials processing, Light Sci. Appl. 3 (390) (2014) 1–12, https://doi.org/10.1038/lsa.2014.30.
[47] P.T. Mannion, J. Magee, E. Coyne, G.M. O'Connor, T.J. Glynn, The effect of damage accumulation behaviour on ablation thresholds and damage morphology in ultrafast laser micro-machining of common metals in air, Appl. Surf. Sci. 233 (1–4) (2004) 275–287, https://doi.org/10.1016/j.apsusc.2004.03.229.
[48] B.N. Chichkov, C. Momma, S. Nolte, F. von Alvensleben,A. Tünnermann, Femtosecond, picosecond and nanosecond laser ablation of solids, Appl. Phys. A: Mater. Sci. Process., 115 (1996) 109–115. https://doi.org/10.1007/BF01567637.
[49] C. Momma, B.N. Chichkov, S. Nolte, F. von Alvensleben, A. Tünnermann, H. Welling, B. Wellegehausen, Short-pulse laser ablation of solid targets, Opt. Commun. 129 (August 1996) 134–142.https, https://doi.org/10.1016/0030-4018(96)00250-7.
[50] D.V. Tran, Y.C. Lam, B.S. Wong, H.Y. Zheng, D.E. Hardt, Quantification of thermal energy deposited in silicon by multiple femtosecond laser pulses, Opt. Express 14 (20) (2006) 9261, https://doi.org/10.1364/oe.14.009261.
[51] R. Stoian, D. Ashkenasi, A. Rosenfeld, E.E.B. Campbell, Coulomb explosion in ultrashort pulsed laser ablation of al 2 o 3, Phys. Rev. B 62 (2000) 13167–13173, https://doi.org/10.1103/PhysRevB.62.13167.
[52] A. San-Blas, A. Rodriguez, E. Granados, Femtosecond laser microprocessing and generation of periodic surface structures: applications in photonics, Ph.D. thesis, Universidad de Navarra (2022).
[53] R. Fang, A.Y. Vorobyev, C. Guo, Direct visualization of the complete evolution of femtosecond laser-induced surface structural dynamics of metals, Light Sci. Appl. 6 (3) (2017), https://doi.org/10.1038/lsa.2016.256 e16256–7.
[54] G. Dumitru, V. Romano, H.P. Weber, H. Haefke, Y. Gerbig, E. Pflüger. Laser microstructuring of steel surfaces for tribological applications, 2000, https://doi.org/10.1007/s003390051073.
[55] Y. Hirayama, M. Obara, Heat effects of metals ablated with femtosecond laser pulses, Appl. Surf. Sci. 197–198 (2002) 741–745, https://doi.org/10.1016/S0169-4332(02)00403-8.
[56] A.G. Demir, B. Previtali, Additive manufacturing of cardiovascular CoCr stents by selective laser melting, Mater. Des. 119 (2017) 338–350, https://doi.org/10.1016/j.matdes.2017.01.091.
[57] E.G. Gamaly, A.V. Rode, Physics of ultra-short laser interaction with matter: From phonon excitation to ultimate transformations, Prog. Quantum Electron. 37 (5) (2013) 215–323, https://doi.org/10.1016/j.pquantelec.2013.05.001.
[58] B. Rethfeld, K. Sokolowski-Tinten, D. Von Der Linde, S.I. Anisimov, Timescales in the response of materials to femtosecond laser excitation, Appl. Phys. A Mater. Sci. Process. 79 (4–6) (2004) 767–769, https://doi.org/10.1007/s00339-004-2805-9.
[59] R. Weber, T. Graf, P. Berger, V. Onuseit, M. Wiedenmann, C. Freitag, A. Feuer, Heat accumulation during pulsed laser materials processing, Opt. Express 22 (9) (2014) 11312, https://doi.org/10.1364/oe.22.011312.
[60] B. Nie, L. Yang, H. Huang, S. Bai, P. Wan, J. Liu, Femtosecond laser additive manufacturing of iron and tungsten parts, Appl. Phys. A Mater. Sci. Process. 119 (3) (2015) 1075–1080, https://doi.org/10.1007/s00339-015-9070-y.
[61] B. Nie, H. Huang, S. Bai, J. Liu, Femtosecond laser melting and resolidifying of high-temperature powder materials, Appl. Phys. A: Mater. Sci. Process. 118 (1) (2014) 37–41, https://doi.org/10.1007/s00339014-8897-y.
[62] L. Kaden, G. Matthäus, T. Ullsperger, H. Engelhardt, M. Rettenmayr, A. Tünnermann, S. Nolte, Selective laser melting of copper using ultrashort laser pulses, Appl. Phys. A: Mater. Sci. Process. 123 (9) (2017) 1–6, https://doi.org/10.1007/s00339-017-1189-6.
[63] T. Ullsperger, G. Mattäus, L. Kaden, M. Rettenmayr, S. Risse, A. Tünnermann, S. Nolte, Selective laser melting of AlSi40 using ultrashort laser pulses for additive

manufacturing applications, Lasers in Manufacturing Conference 2017, Selective (2017) 1–7.
[64] A.B. Kaligar, H.A. Kumar, A. Ali, W. Abuzaid, M. Egilmez, M. Alkhader, F. Abed, A. S. Alnaser, Femtosecond Laser-Based Additive Manufacturing: Current Status and Perspectives, Quantum Beam, Science 6 (1) (2022), https://doi.org/10.3390/qubs6010005.
[65] M. Pasupathy, J.M. Marín, A. Rivas, I. Iturriza, F. Castro, Effect of the solidification time on the median particle size of powders produced by water atomisation, Powder Metall. 59 (2) (2016) 128–141. http://doi.org/10.1080/00325899.2015.1117693.
[66] M. Groenendijk, J. Meijer, Microstructuring using femtosecond pulsed laser ablation, in: 24th International Congress on Applications of Lasers and Electro-Optics, ICALEO 2005 - Congress Proceedings, 408, 2005, pp. 219–225, https://doi.org/10.2351/1.5060548.
[67] H. Huang, B. Nie, P. Wan, L.-M. Yang, S. Bai, J. Liu, Femtosecond fiber laser additive manufacturing and welding for 3D manufacturing, Laser 3D Manufacturing II 9353 (2015) 93530A. http://doi.org/10.1117/12.2082846.
[68] B. Jaeggi, B. Neuenschwander, M. Schmid, M. Muralt, J. Zuercher, U. Hunziker, Influence of the pulse duration in the ps-regime on the ablation efficiency of metals, Phys. Procedia 12 (2011) 164–171, https://doi.org/10.1016/j.phpro.2011.03.118.
[69] M.J. Matthews, G. Guss, S.A. Khairallah, A.M. Rubenchik, P.J. Depond, W.E. King, Denudation of metal powder layers in laser powder bed fusion processes, Acta Materialia 114 (2016) 33–42. http://doi.org/10.1016/j.actamat.2016.05.017.
[70] L. Kaserer, S. Bergmueller, J. Braun, G. Leichtfried, Vacuum laser powder bed fusion—track consolidation, powder denudation, and future potential, Int. J. Adv. Manuf. Technol. 110 (2020) 3339–3346, https://doi.org/10.1007/s00170-020-06071-6.
[71] M. Mizoshiri, K. Nishitani, S. Hata, Effect of heat accumulation on femtosecond laser reductive sintering of mixed cuo/nio nanoparticles, Micromachines 9 (6) (2018), https://doi.org/10.3390/mi9060264.
[72] M. Ćwikła, R. Dziedzic, J. Reiner, Influence of overlap on surface quality in the laser polishing of 3d printed inconel 718 under the effect of air and argon, Materials 14 (2021), https://doi.org/10.3390/ma14061479.
[73] T.L. Perry, D. Werschmoeller, X. Li, F.E. Pfefferkorn, N.A. Duffie, Pulsed laser polishing of micro-milled ti6a14v samples, J. Manuf. Processes 11 (2009) 74–81, https://doi.org/10.1016/j.jmapro.2009.10.001.
[74] A. Sassmannshausen, A. Brenner, J. Finger, Ultrashort pulse laser polishing by continuous surface melting, J. Mater. Process. Technol. 293 (2021) 117058, https://doi.org/10.1016/j.jmatprotec.2021.117058.
[75] J. Li, Y. Wu, B. Zhou, Z. Wei, Laser powder bed fusion of pure tungsten: Effects of process parameters on morphology, densification, microstructure, Materials 14 (1) (2021), https://doi.org/10.3390/ma14010165.
[76] B. Yürekli, L. Schade, T. Ullsperger, B. Seyfarth, H. Kohl, G. Matthäus, D. Liu, M. Rettenmayr, S. Nolte, Additive manufacturing of binary al-li alloys, Procedia CIRP 94 (2020) 69– 73, 11th CIRP Conference on Photonic Technologies [LANE 2020]. https://doi.org/10.1016/j.procir.2020.09.014.